analytical chemistry

Article

Cite This: *Anal. Chem.* 2019, 91, 3619−3627

pubs.acs.org/ac

Concatenated Catalytic Hairpin Assembly/Hyperbranched Hybridization Chain Reaction Based Enzyme-Free Signal Amplification for the Sensitive Photoelectrochemical Detection of Human Telomerase RNA

Yanxin Chu,[†,§] An-Ping Deng,[*,†] Wenjing Wang,[*,‡] and Jun-Jie Zhu[*,§]

[†]The Key Lab of Health Chemistry and Molecular Diagnosis of Suzhou, College of Chemistry, Chemical Engineering and Materials Science, Soochow University, Suzhou 215123, People's Republic of China

[‡]State Key Laboratory of Agricultural Microbiology, College of Science, Huazhong Agricultural University, Wuhan 430070, People's Republic of China

[§]State Key Laboratory of Analytical Chemistry for Life Science, School of Chemistry and Chemical Engineering, Nanjing University, Nanjing, Jiangsu 210023, People's Republic of China

Supporting Information

ABSTRACT: Human telomerase RNA (hTR), an important biomarker for cancer diagnosis, is the template for the synthesis of telomeric DNA repeats and is found to be 7-fold overexpressed in tumor cells. Herein, we present a photoelectrochemical (PEC) biosensor for hTR detection coupled with a novel amplification strategy based on cascades of catalytic hairpin assembly (CHA) and hyperbranched hybridization chain reaction (HB-HCR). At the electrode surface, thiolated hairpin 1 probes were immobilized on deposited CdS nanoparticles via a Cd−S bond. In the presence of target hTR, a CHA reaction was triggered and the exposing of trigger1 could further initiate an HB-HCR reaction to form abundant hemin/G-quadruplex DNAzymes containing dendritic DNA structure. The DNAzymes' catalytic precipitation of 4-chloro-1-naphthol (4-CN) by H_2O_2 subsequently took place on the surface of the PEC electrode and efficiently suppressed the photocurrent output. Therefore, the change of photocurrent response had a positive linear relationship with logarithmic value of hTR concentration varying from 200 fM to 20.0 nM with a limit of detection (LOD) of 17.0 fM. The LOD for CHA/HB-HCR was about 8.8-fold lower than that of CHA/linear-branched HCR (CHA/LB-HCR) and 547-fold lower than that of CHA. By coupling the feature of high signal amplification capacity for DNA nanotechnology, a prominently stable, reproducible, and selective PEC biosensor was successfully constructed and applied in hTR detection.

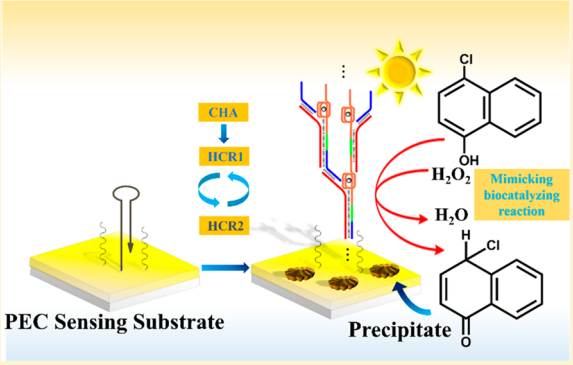

Telomerase is confirmed to be overexpressed in most of the human cancers, proving to be an excellent tumor marker.[1,2] Human telomerase reverse transcriptase and telomerase RNA (hTR) are recognized as two important components of human telomerase.[3,4] Repetitive sequences of TTAGGG are added to the 3′ end of chromosome by telomerase with the aid of its intrinsic RNA template, endowing the cancer cells with indefinite division capability.[5,6] The identification of telomerase activity could be realized either by telomerase reverse transcriptase detection or telomerase RNA detection. Human telomerase RNA is reported to be 7-fold overexpressed in tumor cells by Avilion et al.,[7] providing a valid evidence for the diagnose of cancer by the amount of hTR. Traditional detection methods for hTR include polymerase chain reaction[8] and situ hybridization,[9] which always suffer from the deficiencies such as limited sensitivity, sophisticated instrumentation, and high cost. Therefore, much effort needs to be devoted to develop an alternative method in order to address these limitations.

The photoelectrochemical (PEC) biosensor is recognized as a promising analytical technique and has attracted extensive research attention during recent years due to the outstanding superiorities of easy operation, simple devices, and sensitive detection performance.[10−15] The PEC biosensor utilizes light energy as the input source to excite PEC-active species to generate photocurrent as an output signal, contributing to the extremely low background signal.[16] Moreover, the performance of the PEC biosensor could be easily enhanced by sensitization structures with higher photocurrent conversion efficiency.

Received: December 4, 2018
Accepted: February 8, 2019
Published: February 8, 2019

DOI: 10.1021/acs.analchem.8b05610
Anal. Chem. 2019, 91, 3619−3627

Sensitization strategies such as TiO_2/CdS[17,18] and ZnO/CdS/CdTe structures[12] are widely applied in the biological detection due to their stable chemical properties, unique photoelectrochemical properties, and convenience for modification in the biosensing process. All in all, the PEC biosensor is expected to be an alternative promising approach for the detection of hTR.

On the other hand, the analysis of the low amount of biomarker for a tumor usually requires the involvement of signal amplification. DNA nanotechnology-based signal amplifications, including catalyzed assembly hairpin reaction (CHA),[19−21] hybridization chain reaction (HCR),[22−24] rolling circle amplification (RCA),[25−27] and the cyclic enzymatic amplification method (CEA)[28−30] etc. played significant roles in the amplified detection of various nucleic acids. Among them, the mechanism of CHA and HCR are based on toehold-mediated strand displacement (TMSD) which could be easily generalized to a wide range of nucleic acid targets based on reasonable sequences design.[31] The CHA reaction could be depicted as a series of cascaded assembly reactions triggered and catalyzed by a specific target accompanied by numerous double-helix DNA signal readouts. In a typical HCR process, the recognition of a target initiates the alternating opening of two DNA hairpins to form linear DNA alternating polymeric nanowires,[32,33] while an improved HCR, which is termed as hyperbranched hybridization chain reaction (HB-HCR), could generate multiple hyperbranched DNA polymer nanostructures and has provided an outstanding platform for the exponential signal amplification in bioanalysis.[34−36] In spite of all these advances, the single type of signal amplification strategy, such as CHA, chainlike HCR, HB-HCR, and single-layer cascaded DNA amplification strategy still suffer from limited amplification efficiency.[37−42] Therefore, further rational combination of several of the above-mentioned techniques is expected to provide better biosensing performance.

Herein, we present a label-free PEC biosensing method for hTR detection based on signal amplification of a concatenated CHA/HB-HCR strategy coupled with the high photocurrent conversion efficiency of a TiO_2/CdS sensitization structure and hemin/G-quadruplex DNAzyme catalytic reaction.[43−45] TiO_2 nanoparticles were coated on an indium tin oxide (ITO) electrode to form a mesoporous film as a substrate of cosensitization. CdS nanoparticles were deposited to form the TiO_2/CdS electrode which could further enhance the photocurrent signal and immobilize thiolated hairpin probe 1 (H1). In order to realize the sensitive detection of hTR, an in situ CHA reaction coupled with HB-HCR cascade amplification strategy on the electrode surface was introduced. In the presence of hTR, catalytic DNAzymes-incorporated hyperbranched DNA polymer nanostructures form on the electrode surface and initiate the mimicking biocatalyzing reaction to produce insoluble 4-chloro-1-naphthol (4-CN), forming an insulating barrier on the TiO_2/CdS electrode to inhibit the photocurrent. On the basis of the cooperation of cascaded amplification and mimicking biocatalyzing reaction, the designed PEC biosensing system achieved high selectivity and ultrasensitivity for hTR detection compared with previously reported works.[2,4]

EXPERIMENTAL SECTION

Reagents and Apparatus. The reagents and apparatus used in this work are presented in the Supporting Information.

Nondenaturing Polyacrylamide Gel Electrophoresis (PAGE). The 8% native PAGE was manufactured by mixing 4 mL of deionized water, 2.4 mL of 30% acrylamide/bis(acrylamide) gel solution (29:1), 1.6 mL of 5× TBE buffer, 56 μL of 10% ammonium persulfate (APS), and 8 μL of *N*,*N*,*N*′,*N*′-tetramethylethylenediamine (TEMED). The mixture was loaded in a glue frame and kept still at 25 °C for 30 min. Afterward, 10 μL of each sample together with 2 μL of 6× loading buffer was loaded into the 8% gel for electrophoresis. The PAGE was run at room temperature at 185 V for 40 min. After staining in 2.5 mg/mL (2 μL) ethidium bromide (EB) solution for 15 min, the gels were scanned and imaged using a gel imaging analysis system (WD-9413A, Beijing, China).

Preparation of the PEC Electrode. The TiO_2/CdS PEC electrode was prepared according to the previous report with little modifications.[46] First, the ITO electrode was treated by ultrasonic cleaning with acetone and 1 M NaOH in a water/ethanol mixture (1:1, v/v) in sequence to remove organic matter and hydroxylate the ITO surface for further modification. After washing with water for several times and drying at 80 °C for 12 h, the ITO electrode was coated by homogeneous TiO_2 suspension (20 μL, 1 mg/mL) with an area of 0.25 cm^2, and then annealed at 450 °C for half an hour in a muffle furnace. Afterward, CdS nanoparticles were applied to the TiO_2 surface using ionic layer adsorption reaction (SILAR). Briefly, $Cd(NO_3)_2$ and Na_2S were dissolved in methanol and methanol/water (1:1, v/v), respectively, to obtain 0.1 M stock solutions. Subsequently, the TiO_2-coated ITO electrode was immersed in a $Cd(NO_3)_2$ methanol solution for 1 min and rinsed with methanol. Then, it was dipped in a Na_2S methanol/water solution for 1 min followed by rinsing again with methanol. The two dipping steps composed a cycle of SILAR. After repeating the SILAR cycle for three times to obtain a CdS film, the electrode was dipped into a $Cd(NO_3)_2$ methanol solution, washed with water, and incubated with thiolated H1 for 8 h. Subsequently, the PEC electrode was blocked with 6-mercapto-1-hexanol (MCH) solution (1 mM) and stored at 4 °C for further use.

Enzyme-Free Concatenated CHA and the Hyperbranched HCR Amplification Strategy Procedure. First, the equivalent stoichiometries of oligonucleotides LA and LT we mixed and incubated for 1 h at 37 °C to obtain trigger2. After gel purification, the as-prepared double-stranded substrate was stored at 4 °C for further reaction (for more details see the Supporting Information). DNA probes of annealed H2 and H3 with the concentrations of 1× (2 μM of each probes) and H4, AS1, trigger2, AS2, and SH with the concentrations of 1× (5 μM of each probes) were combined in the above-mentioned order, which were further mixed with different concentrations of target (0 M to 20 nM). The sensing solution was incubated with the prepared PEC electrode at 37 °C for 2 h. After washing with PBS, the electrode was further incubated with a 12 μL aliquot solution containing 6.0 μM hemin and 50 mM KCl for 1 h, and then rinsed with PBS. Subsequently, the catalyzing precipitation reactions caused by G-quadruplex DNAzymes were started by incubating the electrode with 5.0 μL of the precipitation solution containing 0.6 mM H_2O_2 and 1 mM 4-CN for 10 min. Afterward, the electrode was washed with PBS. To investigate the amplification efficiency of the programmed CHA/HB-HCR strategy, CHA/linear-branched HCR (CHA/LB-HCR) cascaded amplification and CHA amplification for contrast were

DOI: 10.1021/acs.analchem.8b05610
Anal. Chem. 2019, 91, 3619−3627

designed, and the procedures of the contrast experiments are presented in the Supporting Information.

PEC Measurement. The PEC measurement was carried out in ascorbic acid (AA, in PBS pH = 7.4, 0.1 M), which served as an the electron donor. A white light with a wavelength from 200 to 2500 nm produced by xenon lamp was used as the excitation source during the measurement. The electrolyte was pumped with nitrogen for 15 min before measurement.

RESULTS AND DISCUSSION

Construction and Characterization of the PEC Electrode. As the biosensing process was constructed on the PEC electrode surface, a stable sensitization structure with high photocurrent conversion efficiency was of prominent importance for the biosensor. In our proposed strategy, TiO_2/CdS was employed. The photogenerated electron−hole transfer mechanism is shown in Scheme 1. TiO_2 can absorb light with the wavelength under 400 nm due to the wide band gap (~3.2 eV), leading to the poor utilization of white light. Compared with TiO_2, the band gap of CdS is 2.4 eV, which can absorb longer-wavelength light. Moreover, the excited electrons can be efficiently transferred from CdS to TiO_2 due to the higher conduction band edge of CdS compared with TiO_2. Therefore, the TiO_2/CdS sensitization structure can dramatically increase the photocurrent conversion efficiency, and promote the photocurrent output signal.

Scheme 1. Schematic Representation of the Photogenerated Electron−Hole Transfer Mechanism

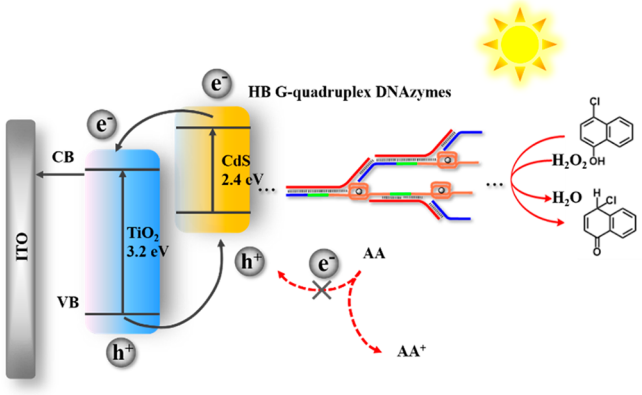

To verify the successful construction of the TiO_2/CdS sensitization structure, we characterized the building process step by step. Figure 1A presents the morphology of the ITO/TiO_2 electrode. TiO_2 film was composed of nanoparticles with size in the range from 22 to 28 nm. After CdS quantum dots were deposited on the surface of the TiO_2 film (Figure 1B), the particles' size increased to 32−40 nm, indicating the successful coating of CdS. The insets for the digital photograph of the ITO/TiO_2 and ITO/TiO_2/CdS electrodes display that the color of the electrode surface changed from white to yellow. The energy-dispersive spectrometry (EDS) characterization of the ITO/TiO_2/CdS electrode is presented in Figure 1C, which also confirmed the existence of Cd, S, and Ti elements. Moreover, the building process of TiO_2/CdS structure was characterized by UV−vis absorption spectra. TiO_2 could only absorb light with a wavelength below 400 nm as shown in Figure 1D, which is determined by the large energy band gap

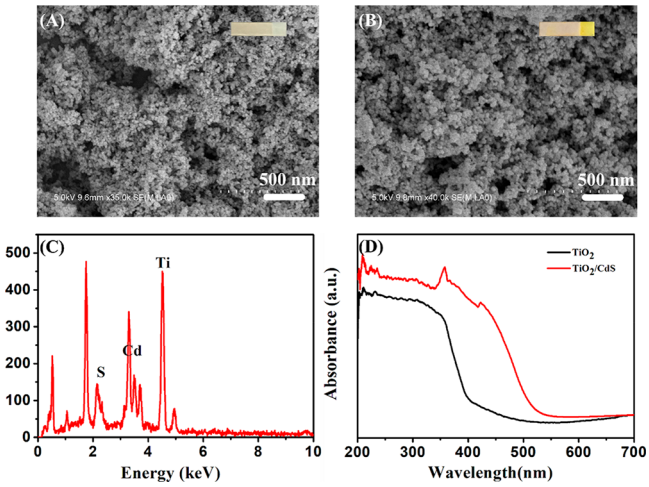

Figure 1. Scanning electron microscopy (SEM) images of (A) ITO/TiO_2 and (B) ITO/TiO_2/CdS. Insets: digital photographs of the corresponding electrodes. (C) EDS characterization of the ITO/TiO_2/CdS electrode. (D) UV−vis absorption spectra of ITO/TiO_2 and ITO/TiO_2/CdS electrodes.

of TiO_2 (~3.2 eV). However, the absorption of TiO_2/CdS extended to 550 nm and had a stronger absorption of below 450 nm, due to the narrow energy band gap of CdS (~2.4 eV), which could make effective use of visible light. All these results suggested the successful fabrication of the proposed PEC electrodes.

Principle of the PEC Biosensor. The signal amplification of the PEC biosensor is mainly based on CHA/HB-HCR cooperating with the mimicking biocatalyzing reaction. The detailed mechanism of the programmed CHA/HB-HCR amplification strategy is illustrated in Scheme 2A. The designed concatenated amplification consisted of eight species which included a superhairpin (SH) and a double-stranded substrate (trigger2). The CHA reaction worked as a sensing module, which could recognize the target analyte and improve the amplification efficiency. The detailed reaction process was as follows: H1 was opened by target to form H1:hTR complex. The mix of H1 and H2 gave rise to the assembly of a duplex (H1:H2 complex), leading to the cyclic reuse of the target along with the CHA products without the assistance of enzyme. Meanwhile, the exposed region of H2 (region 3, 4, 5, 7) could open H3 to form trigger1. Afterward, the resulting trigger1 initiated the HB-HCR reaction. Briefly, the exposed sticky end (region 6*, 7*) on trigger1 conjugated with the toehold (region 6) and opened the duplex of region 7/7* of SH forming an intermediate trigger1:SH complex. In the HB-HCR procedure initiated by the trigger1, the resulting sticky end of SH hybridized with the toehold of H4 (region 11*) and opened H4 to trigger a cascaded hybridization reaction (HCR1). Thus, each trigger1 can propagate an alternating copolymer of SH and H4 (trigger1:$(SH:H4)_n$) which was similar to the linear structure of the traditional HCR product. Meanwhile, the opened loops 8 then acted as a new toehold to initiate a branch migration reaction with assistant strand1 (AS1). Therefore, the SH was further opened, forming a trigger1:$(SH:AS1:H4)_n$ complex. Similarly, the newly exposed sticky region of SH (region 10, 9*) was used to initiate another cascaded hybridization reaction (HCR2) to form the branched structure. The reaction process is described as below: As the double-stranded substrate LT:LA (trigger2) and a single-

DOI: 10.1021/acs.analchem.8b05610
Anal. Chem. 2019, 91, 3619−3627

Scheme 2. Schematic Illustration of the Cascaded CHA/HB-HCR Amplification Strategy (A) and the Building and Biosensing Process of the PEC Biosensor (B)[a]

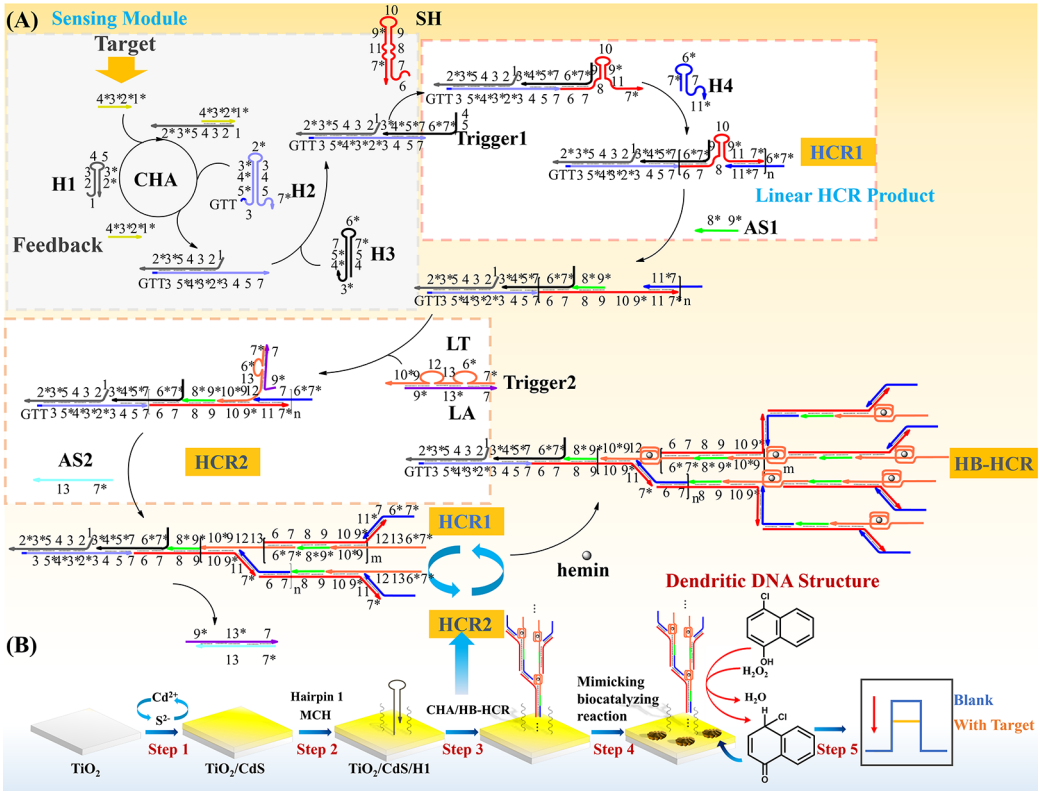

[a]Arrows on DNA strands represent the 3′ terminus.

stranded assistant strand2 (AS2) were employed, the newly exposed sticky region 10 hybridized with the single-stranded overhang of trigger2, leading to a toehold-mediated branch migration reaction that dissociated half of the LA strand from the LT strand. Subsequently, AS2 docked to the last 6 nt of the newly exposed part (region 9*) and finally dissociated the LA strand from the LT strand, resulting in the opening of the second loop. The exposed region 13 functioned as a hemin capture strand, and the sticky end of terminal 5′ of LT was identical to the exposed sticky end of trigger1, reacting with SH to initiate binary growth of the dendritic structure with repeated units of [(SH:AS1: LT):H4]. As a result, a target-triggered assembly of well homogeneous and controlled dendritic DNA structure with numerous intramolecular G-quadruplex DNAzymes was achieved.

The construction and biosensing process of the PEC biosensor are shown in the Scheme 2B. The TiO_2/CdS electrode was prepared by the SILAR method (step 1) as mentioned above. Thiolated hairpin 1 probes were immobilized on deposited CdS nanoparticles on the electrode surface via a Cd−S bond[47] (step 2), and the electrode was further blocked by mercaptoethanol (MCH). In the presence of target, dendritic helix DNA formed on the PEC electrode leading to a remarkable exponential signal amplification. The dendritic DNA could form abundant hemin/G-quadruplex DNAzymes on the surface of the PEC electrode (step 3) and catalyze the precipitation of 4-CN by H_2O_2. The mimicking biocatalyzed reaction led to the generation of insoluble benzo-4-chlorohexadienone to form an insulating layer on the TiO_2/CdS electrode and prevented AA from diffusing to the electrode surface (step 4), resulting in an evident suppression of photocurrent (step 5).

The sequences design of SH and trigger2 played significant roles in the efficiency of signal amplification. IDT DNA Oligo Analyzer and NUPACK were employed to theoretically predict and optimize the diagram of minimum free energy (MFE) structures of the SH and trigger2 (Figure S1), suggesting that their secondary structures and thermodynamic parameters were ideal for further use. Furthermore, a native PAGE of single HB-HCR triggered by initiator (I) was performed to support the design of CHA/HB-HCR. (The detailed mechanism illustration and results are presented in Figures S2 and S3 in the Supporting Information.)

In order to investigate the feasibility of the whole programmable amplification strategy, PAGE was employed first. Eight species of the amplification are presented in lanes 6−9 in Figure 2A and lanes 14−21 in Figure 2B. In the presence of hTR, the band of trigger1 (H1:H2:H3) was observed with a lower migration rate compared with the reaction species (lane 3). The band of trigger1:SH complex with a higher molecular weight could be clearly observed (lane 4 in Figure 2A and lane 10 in Figure 2B). Serial bands of HCR1 and HCR2 products appeared in lane 11 and lane 12, indicating the formation of single structural branches of dendritic DNA structure. In addition, bands of dendritic DNA structure produced by CHA/HB-HCR with lower mobility compared with that of HCR1 and HCR2 were also observed in lane 13. Moreover, the spontaneous interaction between the DNA species without hTR was investigated in lane 14, and the interference of the leakage was within an acceptable limit, indicating the metastable coexistence stability of the DNA

DOI: 10.1021/acs.analchem.8b05610
Anal. Chem. 2019, 91, 3619−3627

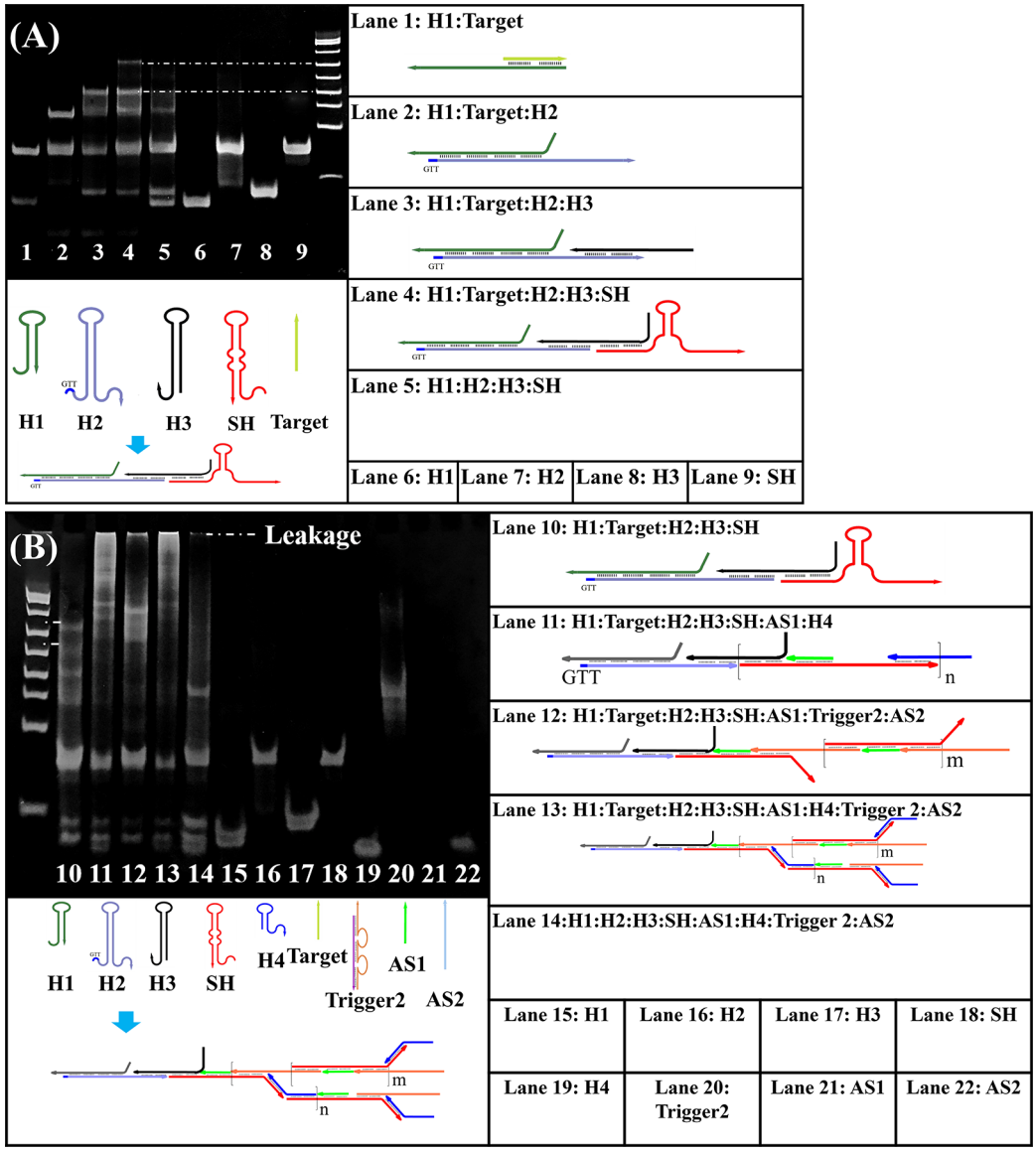

Figure 2. PAGE of CHA amplification (A) and CHA/HB-HCR amplification (B).

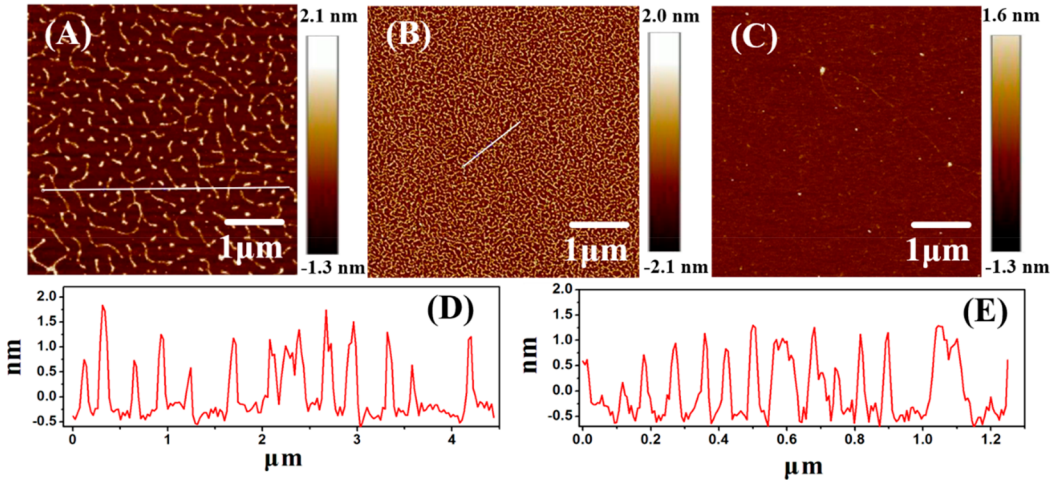

Figure 3. AFM characterization of CHA/L-HCR (A), CHA/HB-HCR (B), and untargeted CHA/HB-HCR reaction (C). (D and E) Cross-sectional profiles of the white lines in panels A and B.

DOI: 10.1021/acs.analchem.8b05610
Anal. Chem. 2019, 91, 3619−3627

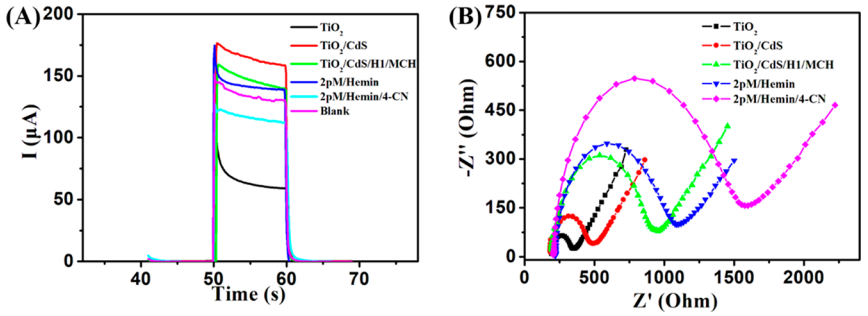

Figure 4. (A) Photocurrent response of the building process of the PEC biosensor. (B) EIS characterization of the PEC biosensor at each step.

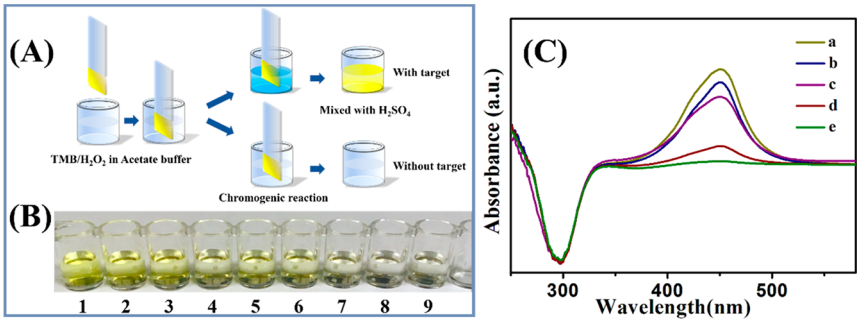

Figure 5. (A) Process of the colorimetric method with hemin/G-quadruplex DNAzymes/TMB/H_2O_2. The digital image (B) and UV−vis absorption spectra (C) of the colorimetric system incubated with different concentrations of hTR. The added concentrations of the hTR in panels C and D are 2 μM for 1, 2, and a, 200 nM for 3,4, and b, 20 nM for 5, 6, and c, 0 M for 7, 8, and d, and TMB in acetate buffer for 9 and e.

probes in the absence of hTR. In Figure S4, the average number of nucleotide bases of the resulting HCR1 (linear HCR, L-HCR) and HB-HCR product was inversely related to the target initiator concentration, which was in high consistence with the reported literature. Altogether, the PAGE results demonstrated the feasibility of the designed concatenated cascade DNA reaction.

The morphology of the designed DNA structures initiated by the hTR was further investigated by atomic force microscopy (AFM). As shown in the Figure 3A, when hTR was incubated with H1, H2, H3, H4, SH, AS1, and H4, linear dsDNA nanowires were observed. By contrast, dendritic structures were achieved when trigger2 and AS2 were added into the L-HCR products (Figure 3B). The yielded alternating copolymer DNA structures appeared to be homogeneous and rigid with a height of 1.5−2.0 nm (Figure 3, parts D and E). The length of the resulting dendritic DNA nanowire structures increased to micrometer long, and some bundles of chains could be observed due to *n*-layer cascaded HCR. In contrast, some small spots instead of assembled product were observed in the absence of hTR (Figure 3C). Thus, the AFM images demonstrated that the designed CHA/HB-HCR behaved as expected, which was consistent to the results obtained by nondenaturing PAGE (Figure 2).

Characterization of the PEC Biosensor. The fabrication process of the biosensor was proved by the PEC characterization. As shown in the Figure 4A, a small photocurrent response (55 μA) was exhibited for the ITO/TiO_2 electrode due to the low photocurrent conversion efficiency of TiO_2. After CdS deposition, the photocurrent response increased to 164 μA due to the formation of a cosensitization structure with TiO_2 which could promote the utilization of visible light. Afterward, the electrode was incubated with sulfhydryl H1, followed by MCH blocking through the strong coupling bond between Cd and S with a photocurrent response decrease of 19 μA. Due to the insulating property of hemin/G-quadruplex DNAzymes, 5 μA decrease of a photocurrent signal was observed after the formation of the dendritic DNA structure/hemin. After the biocatalytic precipitation reaction triggered by 2 pM hTR, an evident PEC signal decrease of 33 μA was observed, which was ascribed to the yielded benzo-4-chlorohexadienone preventing ascorbic acid from diffusing to the electrode surface. Notably, the 15 μA photocurrent decay of the PEC biosensor without target was mainly caused by nonspecific spontaneous interactions between DNA species, which is within the acceptable limit and did not affect the detection of target. This phenomenon is consistent with the results of PAGE (Figure 2). The process of electrode construction was also characterized by electrochemical impedance spectroscopy (EIS) using $[Fe(CN)_6]^{3-/4-}$ as the redox probe. The semicircle at the higher-frequency range of the impedance spectra represented an electron-transfer-limited process which could reflect the value of electron-transfer resistance (R_{et}). As presented by Figure 4B, for the TiO_2-modified ITO electrode, the impedance exhibited a relatively small R_{et}. After CdS deposition, the R_{et} increased, indicating ITO/TiO_2/CdS was successfully obtained. Subsequently, the thiolated H1 and MCH immobilization caused an obvious increase of R_{et} because of the large steric hindrance of DNA and MCH. The impedance value increased after further incubation with hemin, demonstrating the formation of hemin/G-quadruplex DNAzymes on the electrode. Finally, the benzo-4-chlorohexadienone insulating precipitation layer resulted in evident increase of R_{et}.

In order to further verify the feasibility of the mimicking biocatalyzed reaction system on the ITO electrode, a colorimetric method was employed. As shown in the Figure 5A, we dipped the PEC electrode into the well plate with 200

DOI: 10.1021/acs.analchem.8b05610
Anal. Chem. 2019, 91, 3619−3627

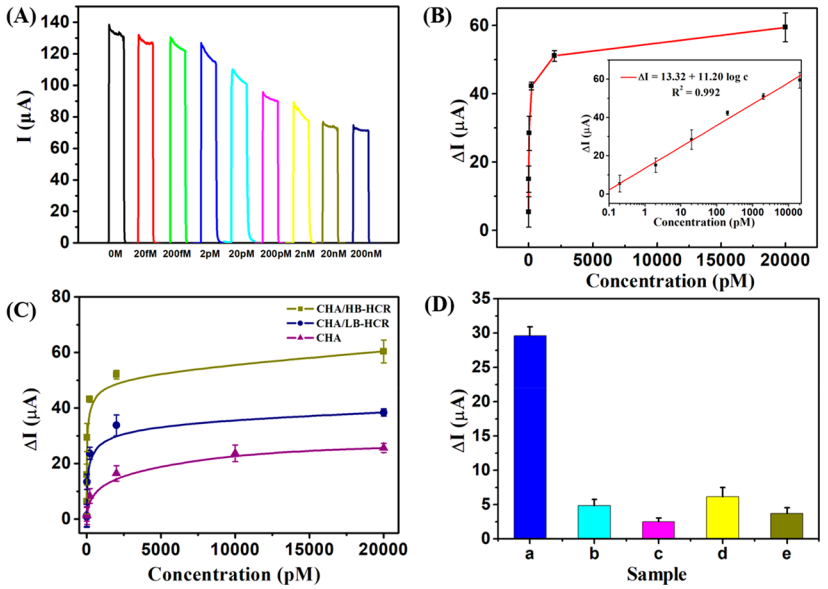

Figure 6. (A) Effect of different concentrations (from 0 M to 200 nM) of hTR on the photocurrent responses. (B) Calibration curve and linear fit curve of the PEC biosensor based on CHA/HB-HCR. (C) Calibration curves of ΔI ($I_{0nM} - I$) of CHA/HB-HCR, CHA/LB-HCR, and CHA amplification. (D) ΔI ($I_{0nM} - I_{20pM}$) of photocurrent response of (a) hTR, (b) SM hTR, and (c) TM hTR in the concentration of 20 pM and (d) SM hTR and (e) TM hTR in the concentration of 100 pM. The error bars illustrated the standard deviations of five replicated tests.

μL of chromogenic substrate solution which contains 3,3′,5,5′-tetramethylbenzidine (TMB, 0.01%, w/v) and H_2O_2 (0.15%, w/v) and quenched the reaction with H_2SO_4 (5%, v/v); the target-triggered hemin/G-quadruplex DNAzymes on the PEC electrode surface could catalyze the substrate to exhibit a color change. As shown in Figure 5B, with the introduction of substoichiometric hTR in the colorimetric system, the color of TMB changed from colorless to yellow; the UV spectra also gave a positive evidence of the formation of hemin/G-quadruplex DNAzymes indicated by the absorption peak at 450 nm (Figure 5C). These results provided sufficient evidence for the construction of the PEC mimicking biocatalyzed reaction sensor system. In conclusion, the results suggested the successful construction of the programmable biosensing system.

Analytical Performance. Under the optimal experiment conditions, the sensitivity of the designed PEC biosensor was confirmed by assaying with different concentrations of hTR. The change of photocurrent response and the logarithmic value of hTR concentration was quasi-linearly related ranging from 200 fM to 20.0 nM (Figure 6B). The limit of detection (LOD) was obtained by plugging the value equal to the signal of blank tests plus 3SD into the regression equation ΔI ($I_{0M} - I$) = 13.32 + 11.20 log C, and the LOD of 17.0 fM is acquired (see the Supporting Information).[48]

To investigate the amplification efficiency of the designed cascaded CHA/HB-HCR approach, CHA/LB-HCR amplification and CHA amplification without HCR were designed for contrast by assaying with a series of hTR concentrations (Figure S5). There was no obvious photocurrent decrease at hTR concentrations below 2 pM using CHA/LB-HCR (Figure S10) and 20 pM using CHA (Figure S7). Moreover, a dramatically higher response of ΔI was produced by the PEC biosensor based on CHA/HB-HCR at the concentration ranging from 0 to 20 nM (Figure 6C). The linear ranges for detection were 2 pM to 20 nM for CHA/LB-HCR with LOD at 151.0 fM and 20 pM to 200 nM for CHA with LOD at 9.3 pM, respectively. The LOD for CHA/HB-HCR was approximately 8.8-fold lower than that of CHA/LB-HCR and 547-fold lower than that of CHA. Therefore, the designed amplification strategy of CHA/HB-HCR makes a remarkable contribution to improve the sensitivity of detection.

Furthermore, the specificity of the designed PEC biosensor was investigated by assaying with hTR, single-base mismatched hTR (SM hTR), and two-bases mismatched (TM hTR) hTR with the same concentration of 20 pM. Small PEC biosensor responses corresponding to SM hTR and TM hTR were observed, which showed negligible difference compared with the blank (Figure 6D). The ΔI ($I_{0nM} - I_{20pM}$) was 29.61 ± 0.64 μA to the hTR at the concentration of 20 pM, 4.83 ± 0.45 μA to SM hTR and 2.45 ± 0.27 μA to TM hTR in response to 20 pM hTR added in the assay, 6.12 ± 0.65 μA to SM hTR and 3.68 ± 0.42 μA to TM hTR in response to 100 pM hTR added, respectively. The cross-reactivities of SM hTR and TM hTR were 16.3% and 8.2%, respectively. This result indicated that a satisfactory selectivity of the biosensor was achieved for hTR detection.

The reproducibility of the proposed PEC biosensor was confirmed by parallel measurement of hTR five times at concentrations of 2, 20, and 200 pM (intra-assay) and the interassay by employing hTR at the same concentration with five electrodes prepared under the same assay conditions. The relative standard deviation values of intra-assay precision and interassay precision are presented in Table 1. On the view of these results, a good reproducibility of the PEC DNA biosensor was achieved.

Table 1. RSD Value of Intra/Interassay Precision at the Concentrations of 2, 20, and 200 pM

concn (pM)	RSD value of intra-assay precision (%)	RSD value of interassay precision (%)
2	3.6	4.4
20	4.3	5.0
200	2.2	2.1

DOI: 10.1021/acs.analchem.8b05610
Anal. Chem. 2019, 91, 3619−3627

To investigate the applicability and reliability of the designed biosensor, we detected hTR in complex biological samples. The complex biological environment was simulated by cell culture media. The results of Table S2 show that the biosensor worked well in the DMEM medium. The photocurrent response had a negative relationship with the concentration of spiked hTR. These results were well consistent with those in PBS, indicating good performance for complex biological analysis for the proposed method.

Finally, we studied the stability for the real application of the biosensor. The ITO/TiO_2/CdS/hairpin1/MCH electrodes were kept at 4 °C for different times, and then assayed with samples at the concentrations of 0 M and 2 pM. As shown in Figure S12A, the photocurrent response for 0 M and 2 pM showed a gradual but slight decrease within a week. After 7 days of storage, the PEC electrodes still retained 85.2% and 89.1% of original PEC signal for 0 M and 2 pM, respectively. As shown in Figure S12B, no significant variation of the photocurrent responses was observed after 10 on/off irradiation repeated cycles incubated with 0 M and 2 pM of hTR. These results showed that the proposed PEC biosensor was stable and has potential for practical application.

CONCLUSIONS

Herein, we proposed a photoelectrochemistry (PEC) biosensor coupled with novel amplification cascades of catalyzed hairpin assembly (CHA) and hyperbranched hybridization chain reaction (HCR) for hTR detection. The photocurrent response has a negative linear relationship with the logarithmic value of hTR concentration ranging from 200 fM to 20.0 nM with an LOD of 17.0 fM. The LOD for CHA/HB-HCR was approximately 8.8-fold lower than that of CHA/LB-HCR and 547-fold lower than that of CHA. The ultrasensitivity of the proposed PEC biosensor is ascribed to the following factors: (1) CHA/HB-HCR with exponential amplification capability provides much higher signal amplification efficiency than the previous one-layer cascaded amplification strategy; (2) the mimicking biocatalyzing reaction could efficiently attenuate the photocurrent response in the presence of target. Taking the superiority of the low background signal of the PEC biosensor and the amplification feature of HB-HCR, the developed PEC biosensing platform exhibited good stability, reproducibility, and specificity and was valid for hTR detection.

ASSOCIATED CONTENT

Supporting Information

The Supporting Information is available free of charge on the ACS Publications website at DOI: 10.1021/acs.analchem.8b05610.

Experimental details, materials and apparatus, photograph images, PEC data, PAGE, and sequences of the oligonucleotides (PDF)

AUTHOR INFORMATION

Corresponding Authors

*E-mail: denganping@suda.edu.cn.
*E-mail: wjwang@mail.hzau.edu.cn.
*E-mail: jjzhu@nju.edu.cn.

ORCID

Yanxin Chu: 0000-0003-0008-2387
An-Ping Deng: 0000-0002-6451-9384
Wenjing Wang: 0000-0003-4035-8552
Jun-Jie Zhu: 0000-0002-8201-1285

Notes

The authors declare no competing financial interest.

ACKNOWLEDGMENTS

We gratefully appreciate funding from the National Natural Science Foundation of China (21603099, 31772053, and 21175097), the International Cooperation Foundation from the Ministry of Science and Technology (2016YFE0130100), and a project funded by the Priority Academic Program Development of Jiangsu Higher Education Institutions (no. YX10900212).

REFERENCES

(1) Luo, S.; Zhang, Y.; Situ, B.; Zheng, L. *Sens. Actuators, B* **2018**, *273*, 853−861.
(2) Wei, Y.; Liu, R.; Sun, Z.; Wang, Y.; Cui, Y.; Zhao, Y.; Cai, Z.; Gao, X. *Analyst* **2013**, *138*, 1338.
(3) Blackburn, E. H.; Epel, E. S.; Lin, J. *Science* **2015**, *350*, 1193−1198.
(4) Xu, J.; Wang, Y.; Yang, L.; Gao, Y.; Li, B.; Jin, Y. *Biosens. Bioelectron.* **2017**, *87*, 1071−1076.
(5) Wu, T.; Zhang, Y.; Hou, T.; Zhang, Y.; Wang, S. *Anal. Chim. Acta* **2018**, *1038*, 120−125.
(6) White, L. K.; Wright, W. E.; Shay, J. W. *Trends Biotechnol.* **2001**, *19*, 114−120.
(7) Avillion, A. A.; Piatyszek, M. A.; Gupta, J.; Shay, J. W.; Bacchetti, S.; Greider, C. W. *Cancer Res.* **1996**, *56*, 645−650.
(8) Heine, B.; Hummel, M.; Demel, G.; Stein, H. *J. Pathol.* **1999**, *188*, 139−145.
(9) Morales, C. P.; Lee, E. L.; Shay, J. W. *Cancer* **1998**, *83*, 652−659.
(10) Fan, G. C.; Zhu, H.; Du, D.; Zhang, J. R.; Zhu, J. J.; Lin, Y. *Anal. Chem.* **2016**, *88*, 3392−3399.
(11) Shen, Q.; Han, L.; Fan, G.; Zhang, J. R.; Jiang, L.; Zhu, J. J. *Anal. Chem.* **2015**, *87*, 4949−4956.
(12) Fan, G. C.; Han, L.; Zhu, H.; Zhang, J. R.; Zhu, J. J. *Anal. Chem.* **2014**, *86*, 12398−12405.
(13) Zang, Y.; Lei, J.; Hao, Q.; Ju, H. *Biosens. Bioelectron.* **2016**, *77*, 557−564.
(14) Qiu, Z.; Shu, J.; Tang, D. *Anal. Chem.* **2018**, *90*, 1021−1028.
(15) Song, Z.; Fan, G. C.; Li, Z.; Gao, F.; Luo, X. *Anal. Chem.* **2018**, *90*, 10681−10687.
(16) Wu, R.; Fan, G. C.; Jiang, L. P.; Zhu, J. J. *ACS Appl. Mater. Interfaces* **2018**, *10*, 4429−4438.
(17) Zhao, M.; Fan, G. C.; Chen, J. J.; Shi, J. J.; Zhu, J. J. *Anal. Chem.* **2015**, *87*, 12340−12347.
(18) Fan, G. C.; Ren, X. L.; Zhu, C.; Zhang, J. R.; Zhu, J. J. *Biosens. Bioelectron.* **2014**, *59*, 45−53.
(19) Chang, C. C.; Chen, C.-P.; Chen, C. Y.; Lin, C. W. *Chem. Commun.* **2016**, *52*, 4167−4170.
(20) Yue, S.; Zhao, T.; Qi, H.; Yan, Y.; Bi, S. *Biosens. Bioelectron.* **2017**, *94*, 671−676.
(21) Liu, S.; Cheng, C.; Gong, H.; Wang, L. *Chem. Commun.* **2015**, *51*, 7364−7367.
(22) Zhang, P.; Wu, X.; Chai, Y.; Yuan, R. *Analyst* **2014**, *139*, 2748−2753.
(23) Yuan, Y.; Liu, G.; Chai, Y.; Yuan, R. *Sens. Actuators, B* **2017**, *246*, 402−407.
(24) Wu, X.; Chai, Y.; Yuan, R.; Zhuo, Y.; Chen, Y. *Sens. Actuators, B* **2014**, *203*, 296−302.
(25) Doerks, T.; Copley, R. R.; Schultz, J.; Ponting, C. P.; Bork, P. *Genome Res.* **2002**, *12*, 47−56.
(26) Han, D.; Wu, C. C.; You, M. X.; Zhang, T.; Wan, S.; Chen, T.; Qiu, L. P.; Zheng, Z.; Liang, H.; Tan, W. H. *Nat. Chem.* **2015**, *7*, 835−841.

DOI: 10.1021/acs.analchem.8b05610
Anal. Chem. 2019, 91, 3619−3627

(27) Yu, N.; Wang, Z.; Wang, C.; Han, J.; Bu, H. *Anal. Chim. Acta* **2017**, *962*, 24−31.
(28) Cui, L.; Lin, X.; Lin, N.; Song, Y.; Zhu, Z.; Chen, X.; Yang, C. J. *Chem. Commun.* **2012**, *48*, 194−196.
(29) Xiao, K.; Liu, J.; Chen, H.; Zhang, S.; Kong, J. *Biosens. Bioelectron.* **2017**, *91*, 76−81.
(30) Wang, M.; Fu, Z. L.; Li, B. C.; Zhou, Y. L.; Yin, H. S.; Ai, S. Y. *Anal. Chem.* **2014**, *86*, 5606−5610.
(31) Zhang, D. Y.; Turberfield, A. J.; Yurke, B.; Winfree, E. *Science* **2007**, *318*, 1121−1125.
(32) Guo, Y.; Wu, J.; Li, J.; Ju, H. *Biosens. Bioelectron.* **2016**, *78*, 267−273.
(33) Dirks, R. M.; Pierce, N. A. *Proc. Natl. Acad. Sci. U. S. A.* **2004**, *101*, 15275−15278.
(34) Chandran, H.; Rangnekar, A.; Shetty, G.; Schultes, E. A.; Reif, J. H.; LaBean, T. H. *Biotechnol. J.* **2013**, *8*, 221−227.
(35) Xuan, F.; Hsing, I. M. *J. Am. Chem. Soc.* **2014**, *136*, 9810−9813.
(36) Bi, S.; Chen, M.; Jia, X.; Dong, Y.; Wang, Z. *Angew. Chem., Int. Ed.* **2015**, *54*, 8144−8148.
(37) Liu, L.; Liu, J. W.; Wu, H.; Wang, X. N.; Yu, R. Q.; Jiang, J. H. *Anal. Chem.* **2018**, *90*, 1502−1505.
(38) Wei, J.; Gong, X.; Wang, Q.; Pan, M.; Liu, X.; Liu, J.; Xia, F.; Wang, F. *Chem. Sci.* **2018**, *9*, 52−61.
(39) Wang, H.; Li, C.; Liu, X.; Zhou, X.; Wang, F. *Chem. Sci.* **2018**, *9*, 5842−5849.
(40) Bi, S.; Yue, S.; Wu, Q.; Ye, J. *Chem. Commun.* **2016**, *52*, 5455−5458.
(41) Ge, L.; Wang, W.; Hou, T.; Li, F. *Biosens. Bioelectron.* **2016**, *77*, 220−226.
(42) Gu, Y.; Song, J.; Li, M. X.; Zhang, T. T.; Zhao, W.; Xu, J. J.; Liu, M.; Chen, H. Y. *Anal. Chem.* **2017**, *89*, 10585−10591.
(43) Gan, C.; Wang, B.; Huang, J.; Qileng, A.; He, Z.; Lei, H.; Liu, W.; Liu, Y. *Biosens. Bioelectron.* **2017**, *98*, 126−133.
(44) Bai, S.; Wang, T.; Zhang, Z.; Sheng, S.; Yu, W.; Xie, G. *Sens. Actuators, B* **2017**, *239*, 447−454.
(45) Zhang, K.; Lv, S.; Lin, Z.; Tang, D. *Biosens. Bioelectron.* **2017**, *95*, 34−40.
(46) Zhang, M.; Xu, Y.; Gong, Z.; Tao, J.; Sun, Z.; Lv, J.; Chen, X.; Jiang, X.; He, G.; Wang, P.; Meng, F. *J. Alloys Compd.* **2015**, *649*, 190−195.
(47) Fan, G. C.; Han, L.; Zhang, J. R.; Zhu, J. J. *Anal. Chem.* **2014**, *86*, 10877−10884.
(48) Fan, G. C.; Zhao, M.; Zhu, H.; Shi, J. J.; Zhang, J. R.; Zhu, J. J. *J. Phys. Chem. C* **2016**, *120*, 15657−15665.

DOI: 10.1021/acs.analchem.8b05610
Anal. Chem. 2019, 91, 3619−3627